Modeling of graphene wrapped indium antimonide nanowire as thermo-optical waveguide

Materials Research
Express

PAPER • **OPEN ACCESS**

Modeling of graphene wrapped indium antimonide nanowire as thermo-optical waveguide

To cite this article: Muhammad Sajid *et al* 2025 *Mater. Res. Express* **12** 036201

Materials Research Express

PAPER

Modeling of graphene wrapped indium antimonide nanowire as thermo-optical waveguide

Muhammad Sajid[1], **Muhammad Zeshan Yaqoob**[1,2], **Majeed A S Alkanhal**[3], **Abdul Ghaffar**[4], **Ahtisham Ali**[5] and **Yasin Khan**[3]

[1] Department of Physics, Government College University, 38000, Faisalabad, Pakistan
[2] Higher Education Department, Government of the Punjab, Lahore, Pakistan
[3] Department of Electrical Engineering, King Saud University, Riyadh, Saudi Arabia
[4] Department of Physics, University of Agriculture, Faisalabad, Pakistan
[5] Department of Electronics and Telecommunications (DET), Politecnico di Torino, Torino, Italy

E-mail: zeeshaan32@yahoo.com

Keywords: drude model, graphene, terahertz, thermo-optical waveguide, indium antimonide, semiconductor

OPEN ACCESS

RECEIVED
23 October 2024

REVISED
28 December 2024

ACCEPTED FOR PUBLICATION
20 February 2025

PUBLISHED
12 March 2025

Abstract

In this research work, the fiber modes supported by the graphene-wrapped indium antimonide nanowire have been examined theoretically. The indium antimonide (InSb) is a semiconductor material, which has temperature-sensitive optoelectronic properties. To model the nanowire of InSb, Drude's model has been used for better results. The Kubo's formalism based on the random phase approximation is used for the modeling of graphene. The impedance boundary conditions (IBCs) are used to compute the characteristic equations. The real and imaginary part of permittivity of InSb as function of THz frequency under different values of temperature $T \in [200\ \text{K},\ 400\ \text{K}]$ has been computed. It is reported that the InSb shows the temperature dependent metal-insulator phase transition i.e., for temperature $T \leqslant 200$ K it behaves as insulator and for $T > 200$ K it acts as metal. The numerical results for dispersion relation, propagation band, propagation losses, cut off frequency range, effective mode index and field profiles have been presented for insulator as well as metallic phase of InSb. Moreover, the impact of chemical potential, radius, and temperature on fiber mode characteristics has been analyzed. The computed numerical results can be applied for designing tunable temperature assisted nano waveguides, thermo-optical sensing probes, thermal imaging and near-field communication devices in THz frequency range.

1. Introduction

Terahertz (THz) technology has emerged as a critical frontier in modern scientific research and applications, bridging the gap between microwave and infrared frequencies [1]. The unprecedented characteristics of THz radiation enable a wide range of applications including ultrafast wireless communication, biomedical imaging, and advanced sensing technologies [2, 3]. The study of the THz waves has become a crucial element in research and development sector of the industries for the manufacturing of the efficient THz devices for the ultra-fast transmission and next generation imaging technologies [4, 5]. The waveguides playing a crucial role in the development of next generation THz technology by providing the active manipulation and control on the THz signals. These structures play a crucial role in directing THz waves with minimal loss and distortion, allowing for efficient transmission through different mediums. Several waveguide designs have been created, such as metallic, dielectric, and photonic crystal waveguides, each tailored to enhance the propagation properties of THz radiation [6–9].

Graphene, an allotrope of the carbon with two dimensionality, is the one of the most promising materials for THz waveguides due to its outstanding electrical and optical characteristics [10, 11]. Graphene integrated waveguide designs have unlocked new possibilities for THz applications, enabling active tuning and improved signal manipulation [12]. Studies have shown that graphene-based plasmonic waveguides offer low loss and

tunability, facilitating efficient signal transmission at THz frequencies [13, 14]. Moreover, researchers have investigated the combination of graphene with different semiconductor materials to develop hybrid waveguide systems, offering enhanced performance and new functionalities [15, 16].

Many studies have been carried out regarding the graphene-based nanowires as waveguides i.e., Gao *et al* developed the theoretical formulation for the plasmon supported by the graphene coated dielectric nanowire (GNW) and discussed the characteristics of plasmon modes. They reported that the properties of the plasmon modes can be tuned by varying the radius of the nanowire, the dielectric permittivity, and the chemical potential of graphene [17]. To get the deeper physical insights, Gao *et al* conducted simulations of the plasmon waveguide modes supported by graphene-coated nanowires (GNWs) using the finite element method (FEM) in COMSOL and they computed the dispersion relation and propagation length, derived the number of supported modes and the single-mode condition from an analytical model, and analyzed the characteristics of the GNW by varying the graphene Fermi level [18]. To realize the reported work, the Chen *et al* fabricated the graphene coated ZnO by using a tape-assisted transfer method under micromanipulation. The enhanced strong surface optical feeds have been reported due to their deep-subwavelength diameter and the high index contrast of the ZnO nanowires. They measured the absorption of up to 0.11 dB/μm in a 606-nm-diameter GZN at a wavelength of 1550 nm. Furthermore, they observed the transmission modulation for a 1550 nm signal using a 590 nm-diameter GZN, indicating the potential of GZN waveguides as nanoscale building blocks for nanophotonic devices [19]. Gao *et al* expanded upon this research by investigating the nonlinear plasmonic coupling effects between closely spaced graphene-coated nanowires (GNWs). They found that the routing of plasmons is sensitive to the input power delivered to the GNWs and is influenced by the third-order conductivity of the graphene layer. Their findings provide insights for designing tunable nanoplasmonic circuits using low-loss, edgeless cylindrical graphene waveguides [20]. Yu *et al* investigated the detailed dispersion analysis of the graphene-coated semiconductor nanowire and computed the proper and improper propagating modes in the terahertz frequency range and classify them into trapped surface waves, fast and slow leaky waves, and surface plasmons [21]. Golestanizadeh *et al* carried out the theoretical investigations on the acoustic plasmons supported by the semiconductor nanowire of indium antimonide (InSb) and its dimmer under the frame work of hydrodynamic model. They have analyzed that the unlike metals, semiconductors often require consideration of two or more types of plasma to accurately describe their plasmonic behavior. A significant increase in the extinction cross-section and field enhancement associated with acoustic localized surface plasmon resonance has been observed [22]. Zhou *et al* demonstrated the potential applications of the InSb nanowires for plasmonic waveguides and real space imaging under external condition. This study performed a comparative analysis of various materials-specifically Ag, graphene, hexagonal boron nitride (hBN), carbon nanotubes (CNTs), tungsten diselenide (WSe2), and InAs nanowires-in terms of their damping ratios and confinement factors for plasmonic waveguiding applications. The results indicate that InAs exhibits greater potential for tuning plasmonic waveguides, offering high confinement and low propagation losses, making it a more favorable candidate compared to other noble metals and 2D materials [23].

This study aims to theoretically model graphene-wrapped InSb nanowires for use as thermo-optical waveguides. InSb's optoelectronic properties, which are highly sensitive to temperature, make it an attractive candidate for terahertz applications [24, 25]. The Graphene enables the active tunability for the THz waves in the optoelectronic devices [26, 27]. To get the active control over the propagation characteristics on the THz radiations, the use of graphene in for the InSb waveguides has been motivated. Moreover, the Indium antimonide (InSb) is a temperature sensitive material and shows the temperature assisted metal insulator transition [28, 29]. Therefore, the theoretical study on the propagation characteristics of THz waves in the graphene coated InSb nanowires under different temperature has been carried out. The present research work has been conducted to achieve the following objectives i.e., (i) To compute the waveguide modes supported by the graphene wrapped InSb nanowire for THz region, (ii) To analyze, how chemical potential, frequency, and external temperature affect the propagation characteristics of waveguide modes and (iii) To summarize the comparative analysis of waveguide modes in InSb, considering its roles as both an insulator and a conductor.

The manuscript is structured as follows: section 2 presents the mathematical details of the analytical modeling of the warped graphene InSb nanowire as a waveguide, while section 3 discusses the numerical results and their implications. Finally, the conclusions drawn from these findings are provided in the last section.

2. Analytical formulations and methodology

The mathematical modeling of the graphene-wrapped InSb nanowire as thermo-optical waveguide has been presented in this section. The waveguide is considered to be directed along the z-axis as depicted in the figure 1. The propagation of the wave guided modes have been considered along the z-direction. The radius of the graphene wrapped InSb nanowire is considered as $r = a$. The region $r > a$ is considered as free space while the

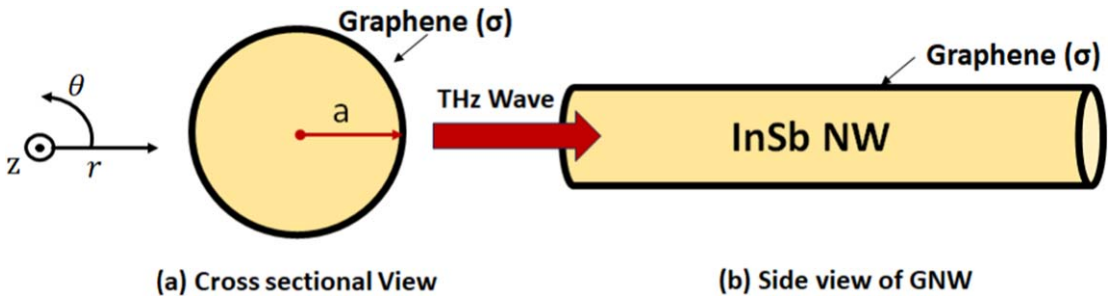

Figure 1. Schematic view of graphene wrapped InSb NW based thermo-optical waveguide.

$r < a$ is taken as InSb nanowire and the graphene has been considered as negligible thickness at $r = a$ with a conductivity (σ_g). The conductivity of the graphene has been modeled in the frame work of semi-classical Kubo's formalism and expressed in terms of incident frequency (ω), temperature (T), chemical potential (μ_c), scattering rate (τ), Boltzmann constant (K_B) and reduced plank's constant ($\hbar$) as,

$$\sigma_g = i\frac{e^2 K_B T}{\pi^* \hbar^2 \left(\omega + \frac{i}{\tau}\right)}\left(\frac{\mu_c}{K_B T} + 2\ln\left[e^{-\frac{\mu_c}{K_B T}} + 1\right]\right) + i\frac{e^2}{4\pi\hbar}\ln\left(\frac{2\,|\mu_c| - \hbar\left(\omega + \frac{i}{\tau}\right)}{2\,|\mu_c| + \hbar\left(\omega + \frac{i}{\tau}\right)}\right) \tag{1}$$

where the terms ω, μ, T, k_B, τ and $\hbar$ stands for the incident frequency, chemical potential, temperature, Boltzmann constant, scattering rate and reduced plank's constant respectively [11–13]. This model assumes an idealized isotropic graphene layer, however the specific chirality configurations, such as zigzag and armchair edges, can influence the local electronic structure of graphene. To simplify the problem, the variation in the chirality configuration has not been added. For the structure considered in this study, the influence of armchair and zigzag chirality is minimal due to the wavelength of THz waves being much larger than the diameter of the nanowire. In this regime, the electromagnetic response of the graphene-wrapped InSb nanowire is predominantly governed by its macroscopic properties rather than the atomic-scale edge configurations. Consequently, the armchair and zigzag configurations are expected to behave similarly, with negligible differences in their impact on the propagation characteristics of the waveguide modes. The modeling of the indium antimonide (InSb) in the terahertz frequency range has been done by using the Drude model as follows [28, 29]:

$$\varepsilon_T = \varepsilon_\infty - \frac{\omega_p^2}{\omega^2 + i\gamma\omega} \tag{2}$$

where ε_∞ denotes high permittivity frequency, γ is damping constant, ω_p denotes plasma frequency with expression $\omega_p = \left(\frac{N(T)e^2}{\omega\, m^*}\right)^{\frac{1}{2}}$, where the m^* is effective mass of free charge carriers and 'N(T)' is the temperature dependent charge carrier density and 'e' represents the value of electronic charge.

To solve the mathematical problem, the Maxwell's equations have been utilized to compute the wave equations with respect to each region. For the present work, the fundamental guided modes supported by graphene wrapped InSb NW based thermo-optical waveguide have been computed for the transverse magnetic (TM) polarization. The nanowire has been modeled as cylindrical shaped road. To attain the symmetry in the mathematical equations, the waveguide modes has been formulated in the frame work of cylindrical coordinates (r, θ, z). The guided modes in the frame work of the cylindrical coordinates are used to solve the equation satisfying **E** and **H** fields. An expression for the electric and magnetic field is be computed. In cylindrical coordinate (r, θ, z) an overall solution to the vector wave equation for source-free and lossless media by the wave equation as [17, 18]

$$(k^2 - \beta^2)E_r = i\beta\frac{\partial E_z}{\partial r} \tag{3}$$

$$(k_i{}^2 - \beta^2)H_\theta = i\omega\varepsilon_i\frac{\partial E_z}{\partial r} \tag{4}$$

Depending on whether $k_i{}^2 - \beta^2$ positive or negative, Fiber mode $k_2 < \beta < k_1$, Plasmon modes $\beta > k_1$, k_2

$$(k_i{}^2 - \beta^2)E_r = i\beta\frac{\partial E_z}{\partial r} \tag{5}$$

where the k_i corresponds to wavenumber of the respective region with i = 1, 2. The solution of the above equations has been solved analytically to compute the electromagnetic modes in for the both regions i.e., inside

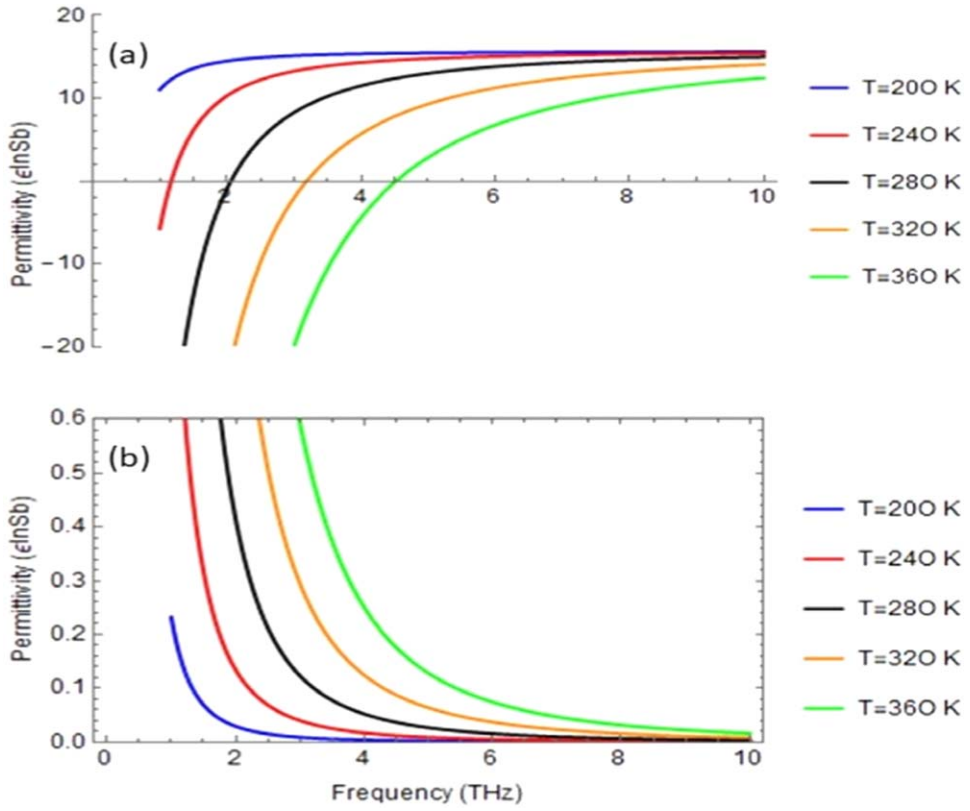

Figure 2. Modeling of the permittivity of InSb as a function of THz frequency: (a) Real part (b) Imaginary part with $\varepsilon_\infty = 15.68$, $\gamma = \pi * 10^{11}$ rad s^{-1} &Eg $= 0.26$ eV.

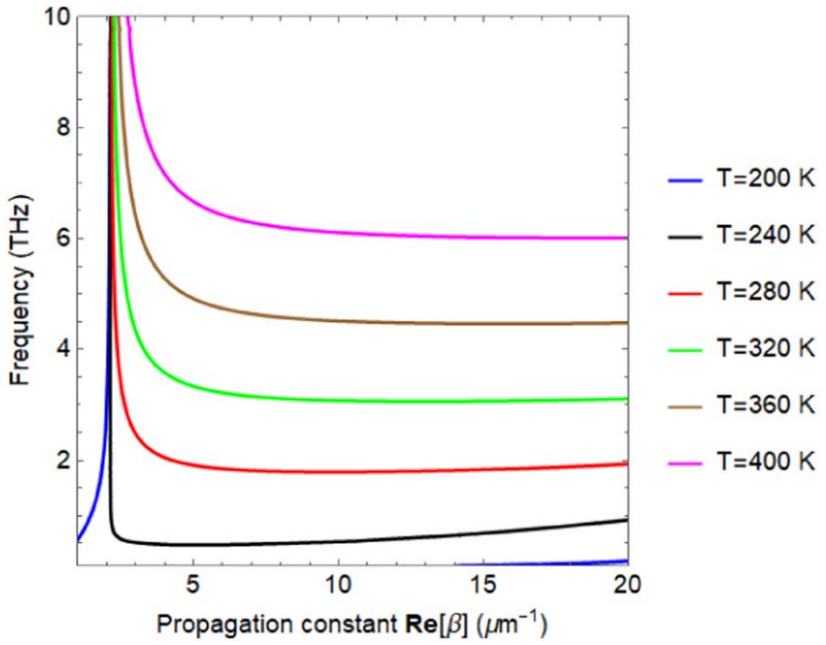

Figure 3. Dispersion relation for various temperature at a constant radius of graphene wrapped InSb NW.

the graphene-wrapped InSb NW ($r < a$) and

$$E_z = AJ_0(\gamma_1 r) \tag{6}$$

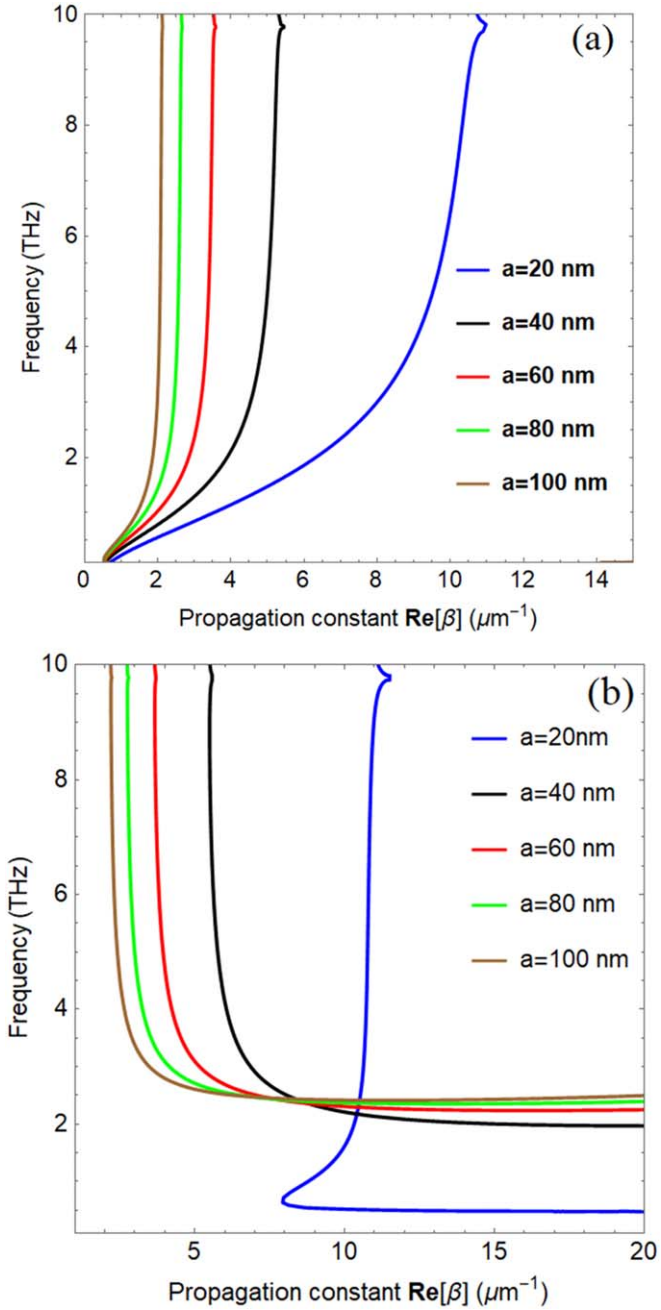

Figure 4. Dispersion relation for various values of diameter of graphene wrapped InSb NW (a) T = 200 K (b) T = 300 K.

$$E_r = \frac{i^*\beta^*A}{(k_1{}^2 - \beta^2)}\frac{\partial J_0(\gamma_1 r)}{\partial r} \tag{7}$$

$$H_\theta = \frac{i^*\omega^*\varepsilon_T{}^*A}{(k_1{}^2 - \beta^2)}\frac{\partial J_0(\gamma_1 r)}{\partial r} \tag{8}$$

outside the graphene-wrapped InSb NW ($r > a$) as

$$E_z = B \quad K_0(\gamma_2 r) \tag{9}$$

$$E_r = \frac{i^*\beta^*B}{(k_2{}^2 - \beta^2)}\frac{\partial K_0(\gamma_2 r)}{\partial r} \tag{10}$$

$$H_\theta = \frac{i^*\omega^*\varepsilon_o{}^*B}{(k_2{}^2 - \beta^2)}\frac{\partial K_0(\gamma_1 r)}{\partial r} \tag{11}$$

In the equations above, 'A' and 'B' represent the unknown coefficients corresponding to the fields in the regions $r < a$ and $r > a$ respectively. By applying the boundary conditions at the interface $r = a$, on the E & H fields as provided in [11, 12]

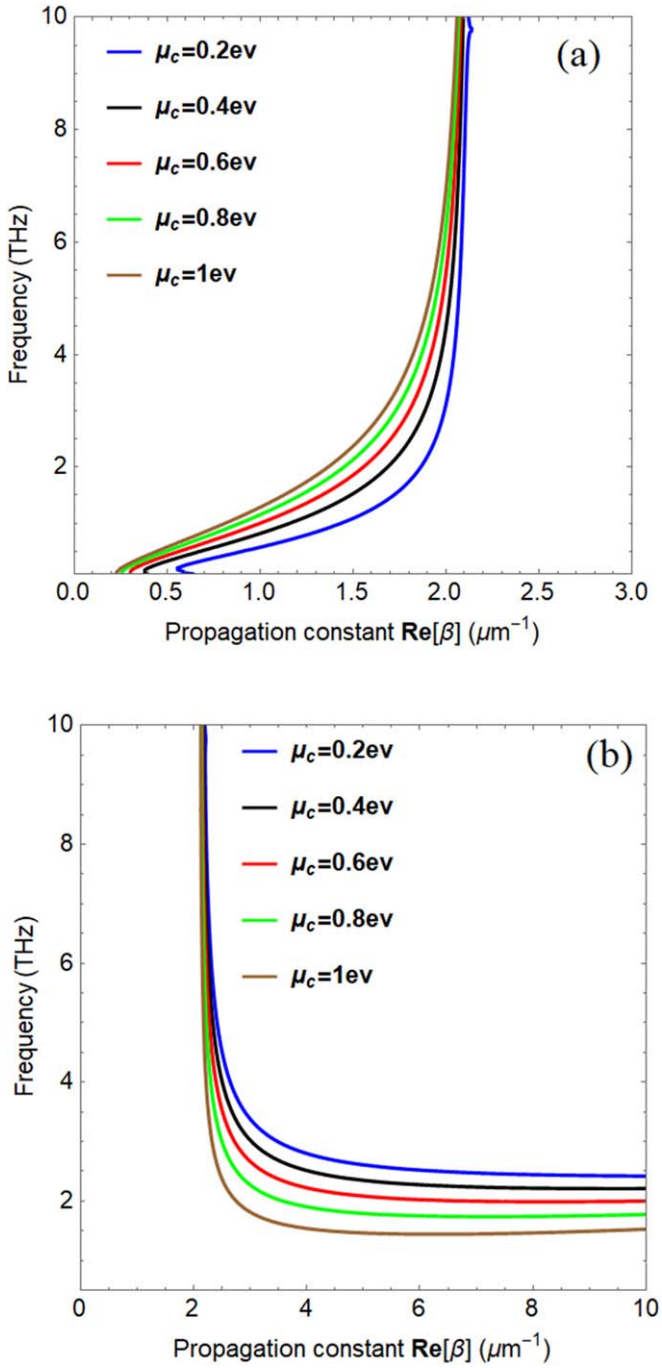

Figure 5. Dispersion relation for various values of chemical potential of graphene wrapped InSb NW (a) T = 200 K (b) T = 300 K.

$$\left.\begin{aligned} E_z|^{+} &= E_z|^{-} \\ H_\theta|^{+} - H_\theta|^{-} &= \sigma_g\, E_z| \end{aligned}\right\} \tag{12}$$

The notations in the above boundary conditions stands for '+' mean $r > a$ External and '−' mean $r < a$ internal. By applying boundary conditions [12, 28]

$$\frac{\varepsilon_T J_1(\gamma_1 a)}{\gamma_1 J_0(\gamma_1 a)} + \frac{\varepsilon_o K_1(\gamma_2 a)}{\gamma_2 K_0(\gamma_2 a)} = \frac{i\sigma_g}{\omega} \tag{13}$$

where the (J_1, J_0) and (K_1, K_0) stands for the Bessel functions and modified Bessel functions of first order and zero order respectively. The computed characteristics equation provides the mathematical solution of the wave guides modes by the graphene wrapped InSb nanowire. To get the physical insight, a detailed numerical solution has been presented in the subsequent section.

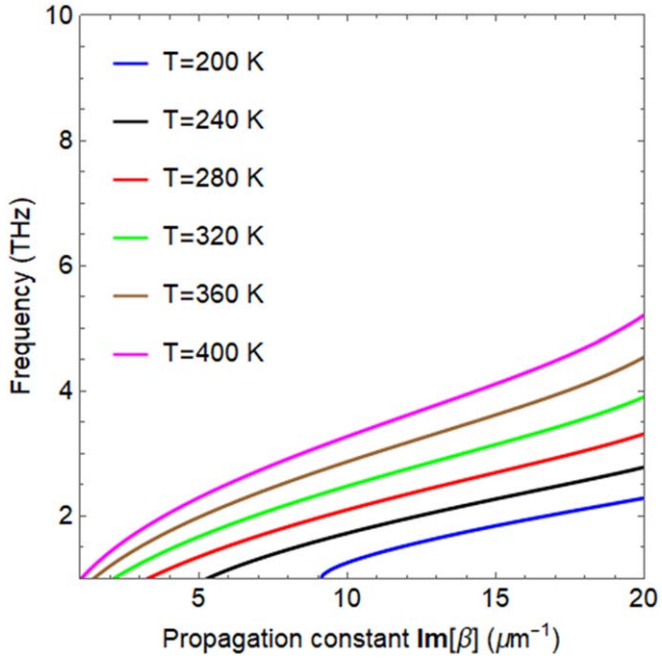

Figure 6. Propagation losses as a function of frequency for various temperatures of a graphene-wrapped InSb NW.

3. Results and discussion

The propagation characteristics of graphene based thermo-optical waveguide in the THz range have been presented in this section. In the first part, the temperature sensitive modeling of the InSb nanowire in THz range has been presented in detail while in the second part, the propagation characteristics of waveguide modes have been discussed in detail.

3.1. EM modeling of InSb nanowire as temperature sensitive material

Figure 2 illustrates the real and imaginary components of the relative permittivity of InSb as a function of THz frequency, with variations in temperature. The permittivity of InSb is calculated using the Drude model, as described in equation (2). The temperature dependent charge carrier density "N(T)" is computed as $N = 5.76 \times 10^{20} T^{\frac{3}{2}} \exp(-\frac{E_g}{2k_B T})$, where E_g is the energy bandgap, T is temperature in Kelvin and k_B is the Boltzmann constant. The graphs for ε_T are presented for the temperature range of 200 K to 400 K. It is evident that the real part transitions from positive to negative as the temperature increases from 200 K to 360 K. This indicates that InSb behaves as an insulator at T = 200 K, whereas for temperatures above 200 K, it exhibits conductive behavior [25, 29].

3.2. Characteristics of thermo-optical waveguide

The fiber modes supported by the thermo-optical waveguide based on the graphene wrapped InSb nanowire have been computed. The characteristics equation (13) has been solved numerically in the frame work of the Wolfram Kernel in Mathematica software pack. To compute the roots of the characteristic equation, the contour plot technique has been implemented in the kernel. The propagation characteristics of the waveguide modes, propagation band, threshold frequency, propagation losses, damping effects, effective mode index and electric field profiles have been computed. Further the influence of temperature, radius of the waveguide and chemical potential of the graphene has been analyzed for all the computed results. To compute the propagation band and threshold frequency of waveguide modes supported by the graphene wrapped InSb nanowire, the dispersion curves in relation with frequency (f) and Re(β) have been computed. Further, the influence of the temperature (T), chemical potential (μ_c) and radius of waveguide has been analyzed and presented in the figures 3–4.

The figure 3 depicts the dispersion curve for the waveguide modes under the temperature variation $T \in [200,\ 240,280,320,\ 360,\ 400]K$. It is obvious from the figure that the with the increase of the temperature, the propagation frequency and band gap increase. The possible reason for this trend is the increase of the plasma frequency (ω_p) of InSb with the increase of temperature. Further, it is important to note that the trend of the dispersion curve is same for the temperature 240 K to 400 K but for T = 200 K the trend is opposite. The major reason for such trend is temperature sensitive behavior of the InSb i.e., for the T = 200 K, the InSb

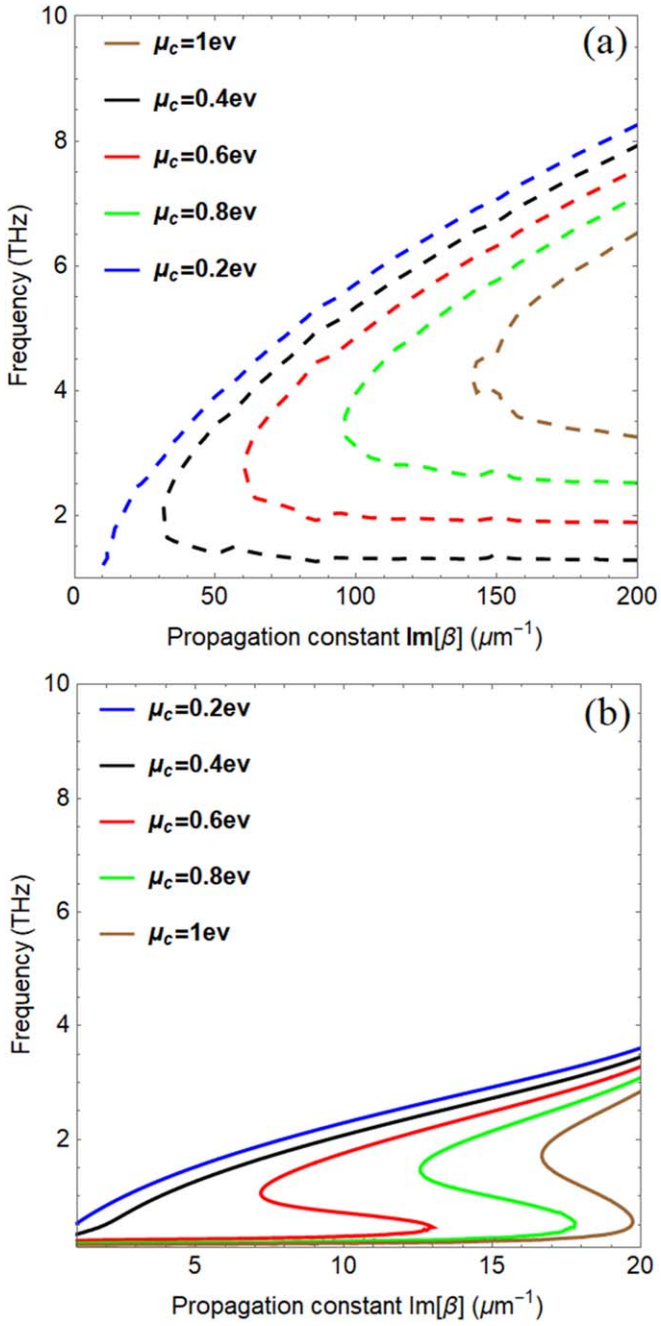

Figure 7. Propagation losses as a function of frequency for under different values of chemical potential of graphene for graphene wrapped InSb NW (a) T = 200 K (b) T = 300 K.

behave as insulator while for the T > 200 K it behaves as conductor, as explained in the figure 2. To analyze the two distinct nature of waveguide modes viz., InSb as insulator (T = 200 K) and InSb as conductor (T = 300 K), the comparative analysis of the results has been shows in figures 5 and (5) for the different values of chemical potential and radius respectively.

In figure 5 the influence of the chemical potential (μ_c) on the propagation characteristics of the waveguide mode has been presented for the different values i.e., μ_c = 0.2 eV, 0.4 eV, 0.6 eV, 0.8 eV & 1.0 eV. The figure 5(a) delas with the waveguide modes supported by the graphene-wrapped InSb NW for T = 200 K while the figure 5(b) presents the waveguide modes for T = 300 K. It can be analyzed that the modes are quite opposite to each other. The waveguide modes under T = 200 K, the graphene wrapped InSb as insulator, the propagation constant shifting towards the lower values with the increase of chemical potential and the speed of the propagating mode is increases with the increase of chemical potential. However, for the case of InSb as conductor at T = 300 K, the propagation frequency starts decreasing towards the lower THz with the increase of chemical potential (μ_c) and the speed of the propagating mode starts decreasing as provided in the figure 5(b).

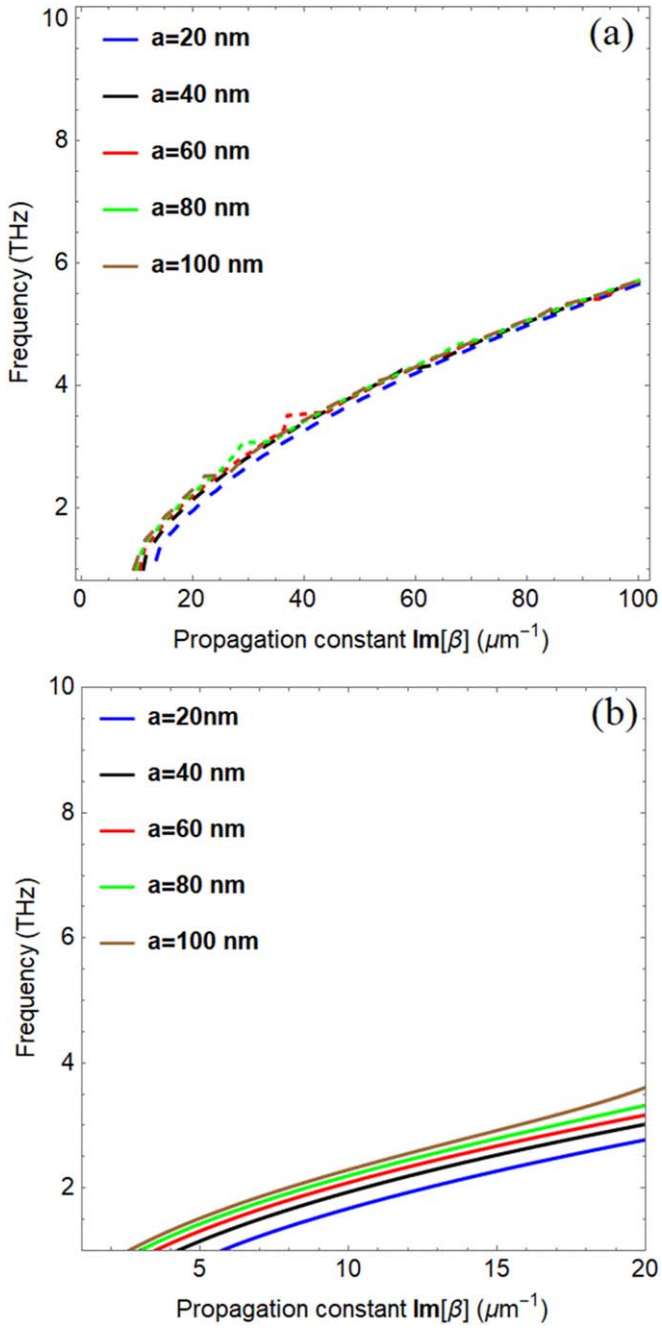

Figure 8. Propagation losses as a function of propagation frequency under different values of radius of graphene wrapped InSb NW based waveguide (a) T = 200 K (b) T = 300 K.

The dimension of the waveguide plays important role in controlling the propagation frequency and cut off frequency. To analyze the propagation characteristics of the waveguide modes as function of structural paraments i.e., the dispersion curves have been plotted under different values of the radius of the graphene wrapped InSb thermo-optical waveguide i.e., a = 20 nm, 40 nm, 60 nm, 80 nm & 100 nm· The influence of the radius of the waveguide on the propagating modes under both configurations i.e., T = 200 K and T = 300 K has been presented in figures 4(a) and (b) respectively. For the case, graphene wrapped InSb nanowire at T = 200 K in figure 4(a) that it is obvious from the figure that the with the increase of the radius of waveguide, the propagation constant (beta) shifting towards the lower value while the propagation frequency band ranges from 1 THz to 10 THz. For the case T = 300 K, it is clear from the figure 4(b) that at the radius a = 20 nm, the propagation mode has the lower cut off frequency while the cut off frequency shifting towards the high THz frequency range as the radius of the waveguide increases.

To estimate the propagation losses and attenuation features of the graphene wrapped InSb waveguide, numerical results between the operating frequency and Im[β] have been plotted under different values of the

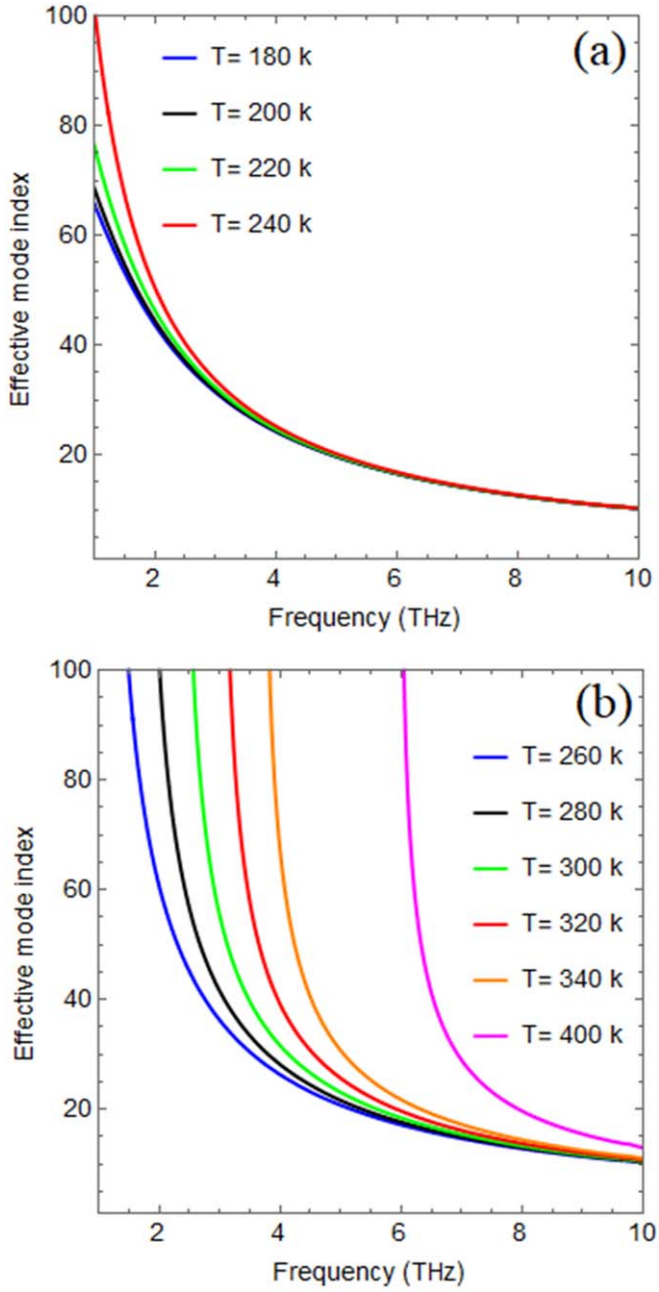

Figure 9. Effective mode index as function of frequency under different values of temperature for graphene wrapped InSb NW based waveguide (a) InSb as insulator (b) InSb as conductor.

temperature i.e. $T \in [200, 240, 280, 320, 360, 400]$ K. From figure 6, it can be concluded that with the increase of temperature, the propagation losses and attenuation increase.

The figure 7 presents the impact of doping level of the graphene i.e., chemical potential (μ_c) on the propagation losses of the waveguide modes under different temperature conditions i.e., T = 200 K and T = 300 K figures 7(a) and (b) respectively. it is clear from the figure 7(a) that the with the increase of chemical potential of the graphene, the losses have been increased significantly as compared to the temperature variation and the second important trend is the propagation loss corresponding to the high frequency values with the increase of chemical poetical (μ_c) as provided in the other works [13, 15, 28]. However, for the case T = 300 K when InSb behave as conducting material, the propagation losses correspond to lower frequency values with the low damping features as compared to the case when InSb behave as Insulator at T = 200 K. Further, it is depicted in the figure 7(b) that with the increase of chemical potential the propagation loss decreases as per corresponding operating frequency. The figure 8 presents the radius dependent propagation loss and damping features of the propagating mode under different values of radius i.e., a = 20 nm, 40 nm, 60 nm, 80 nm & 100 nm. The figure 8(a) provides the physical information about the propagation loss and damping features of waveguide modes as function of operating

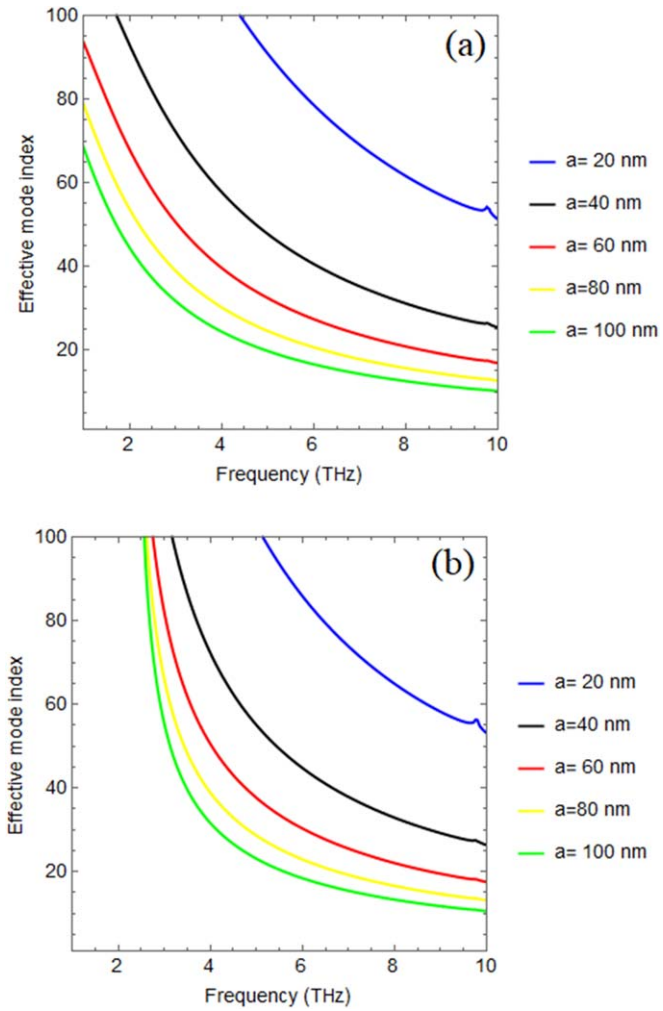

Figure 10. Effective mode index as function of frequency under different values of radius of graphene wrapped InSb NW based waveguide (a) InSb as insulator T = 200 K (b) InSb as conductor, T = 300 K.

frequency for T = 200 K. It can be analyzed from figure that for this case, with the increase of radius of the waveguide the variation in the propagation loss in indelible while for the case of T = 300 K when InSb behave as conductor, the propagation loss increases with the increase of the radius size from a = 20 nm to 100 nm. It is worth noting that the propagation frequency increases along with it.

The effective mode index is very important parameter for the designing and fabrication of the waveguides. It delas with the confinement of the propagating modes within the waveguide with respect to free wavevector (ko) and its explicit mathematical expression is defined as $Re(\beta)/ko$. The numerical results regarding the effective mode index as function of frequency under the variation of temperature (T), chemical potential (μ_c) and radius of waveguide (a) have been presented in figures 9–10 respectively. In figure 9 it has shown that the effective mode index of the waveguide modes as function of the THz frequency under the temperature variation ($T \in [200, 400]$ K) for two phases of the InSb i.e., Insulator phase and conductor phase. It can be deduced from the figure 9(a) that under condition i.e., (InSb as insulator) the effective mode index of the waveguide modes monotonically decreases with the increase of the propagation frequency and for the frequency range (5 to 10) THz the effective mode index corresponds to constant value. Further it is clear that the effective mode index increases with the increase of temperature. In the scenario where InSb realized as a conductor, as illustrated in figure 9(b), the effective mode index diminishes with increasing propagation frequency. Conversely, as the temperature rises, the propagation frequency begins to shift toward higher values, accompanied by a modest increase in the effective mode index.

Figure 11 illustrates the effect of chemical potential on the effective mode index as a function of THz frequency for two states of InSb. The analysis examines various values of the chemical potential in the graphene waveguide, specifically within the range of $\mu_c \in$ (0.2 eV, 0.4 eV, 0.6 eV, 0.8 eV, and 1.0 eV). In the case of T = 200 K, where InSb acts as an insulator, the effective mode index decreases as the chemical potential rises. This reduction is attributed to increased losses associated with the elevated chemical potential of graphene, resulting in lower confinement of

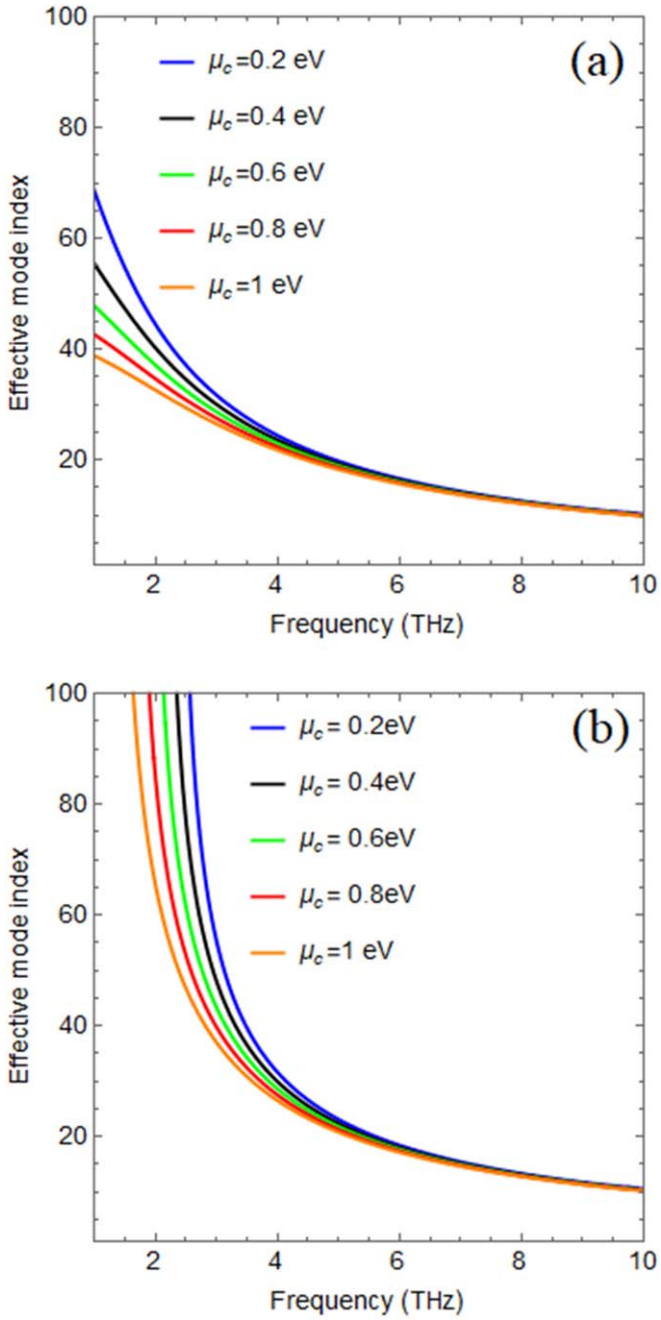

Figure 11. Effective mode index as function of frequency under different values of chemical poetical for graphene wrapped InSb NW based waveguide (a) InSb as insulator T = 200 K (b) InSb as conductor, T = 300 K.

the waveguide modes in the graphene-wrapped InSb nanowire, as shown in figure 11(a). In similar way, the figure 11(b) provides the analysis for impact of the chemical potential on the effective mode index for the case of T = 300 K, where InSb acts as conductor. The figure clearly indicates that as the chemical potential increases, the effective mode index is associated with a reduced propagation band gap. Moreover, in relation to the propagation frequency, the effective mode index exhibits a decreasing trend.

To analyze the dimensional impact on the confinement of the waveguide modes of the graphene wrapped InSb nanowire, the effective mode index has been computed under different values of radius of waveguide i.e., a = 20 nm, 40 nm, 60 nm, 80 nm & 100 nm in figure 10. The effective mode index has been presented for InSb as insulator and conductor in figures (a) and (b) respectively. These figures clearly demonstrate that as the waveguide radius increases, the effective mode index decreases. This trend is further associated with the cutoff frequency of the waveguide, indicating an inverse relationship between waveguide size and propagation frequency. It is worth mentioning that the relationship between the diameter of InSb nanowires and their corresponding bandgap energies has been carefully considered. It is well-documented that quantum confinement effects significantly influence the bandgap energy as the diameter decreases below a critical

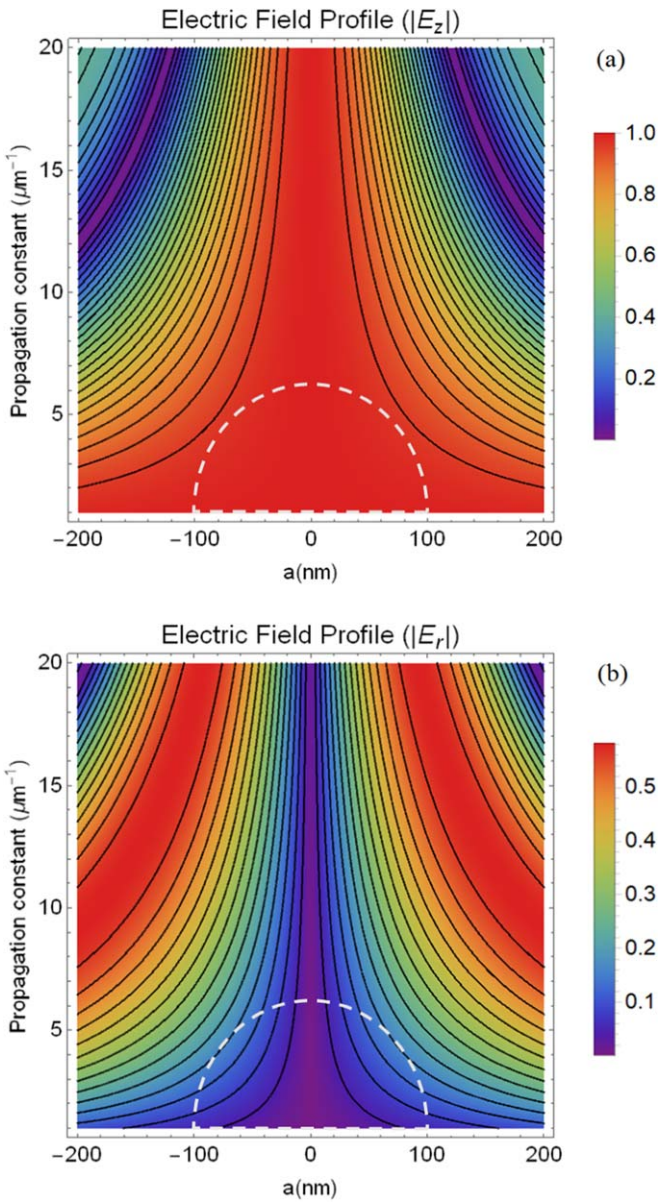

Figure 12. Normalized electric field profiles for the graphene-wrapped InSb NW with 100 nm radius (a) $|E_z|$ and (b) $|E_r|$ at $f = 1$ THz, T = 300 K & $\mu_c = 0.2$ eV.

threshold [30]. For diameters larger than 65 nm, the bandgap energy remains nearly identical to that of the bulk material (0.17 eV) due to negligible confinement effects. However, as the diameter reduces from 65 nm to 30 nm, a modest increase in bandgap energy is observed, ranging from 0.17 eV to 0.20 eV. A more pronounced increase occurs when the diameter decreases further, from 30 nm to 5 nm, with the bandgap energy rising sharply from 0.20 eV to 1.2 eV. These changes in bandgap energy are particularly relevant in the mid-infrared (MWIR) and near-infrared (NIR) regions, enabling InSb nanowires to support multi-spectrum detection. For diameters exceeding 10 nm, the bandgap energies are aligned with MWIR detection, while smaller diameters extend this capability to the NIR region [30, 31]. However, the current study is focused on the THz frequency range, where the optical properties of InSb nanowires are primarily dictated by a temperature-driven phase transition from an insulating to a metallic state. In this regime, variations in bandgap energy due to diameter changes are negligible compared to the dominant thermal effects influencing the optical response. Consequently, size-dependent optical variations are not significant for the parameters under investigation.

In the figure 12, the density plots for the electric field profiles ($|E_z|$ & $|E_r|$) as a function of radial distance (a) and the propagation constant (β) for the graphene-wrapped InSb nanowire waveguide at THz frequencies is presented. The dotted semi-circle in the figs represents cross-sectional view of the NW. From figure 12(a), it can be deduced that the electric field profile is symmetric about the center of the nanowire, indicating a uniform distribution influenced by the cylindrical geometry of the nanowire. It can be analyzed that the field strength $|E_z|$

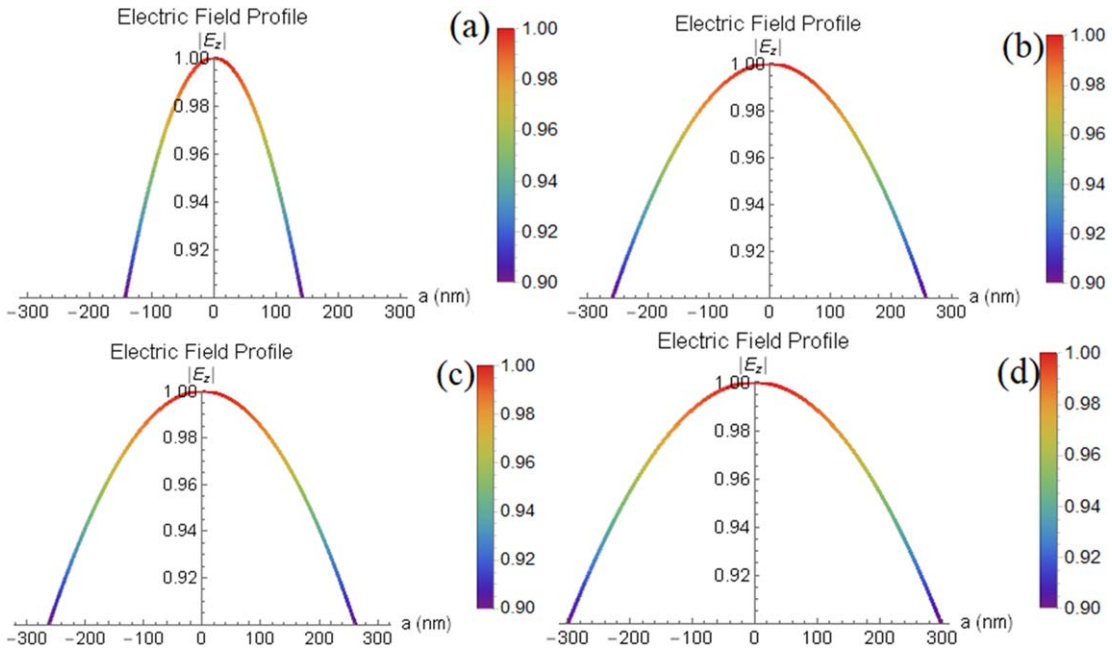

Figure 13. Spatial Field distribution inside and outside of graphene wrapped NW of radius 100 nm (a) At $f = 2.63$ THz, Neff = 81.31 (b) At $f = 4.54$ THz, Neff = 26.24 (c) At $f = 6.57$ THz, Neff = 16.41 (d) At $f = 8.95$ THz, Neff = 11.49.

is maximum at the center and decreases smoothly toward the edges i.e., $a = \pm 100$ nm. This behavior is typical for the fundamental mode in waveguides, where the field is strongest at the core and diminishes in the surrounding medium due to boundary conditions and waveguide confinement. The confinement arises from the unique optical properties of graphene, which include its high conductivity and ability to sustain plasmonic modes at THz frequencies [32]. This allows for effective localization of the electromagnetic field even when the wavelength is much larger than the nanowire dimensions. The strong dependence of the field distributions on the propagation constant (β) is evident in the results. Larger values of β are associated with enhanced confinement of the field within the nanowire core. This is a direct result of the proportionality between β and the effective mode index, which increases with greater field localization. The radial component of the electric field ($|E_r|$) for the waveguide is depicted in figure 12(b). It is evident that the radial electric field is minimal at the center of the waveguide and reaches its maximum at the edges. This suggests that the radial component of the electric field is weakly confined at the core of the waveguide. As the radius increases, the magnitude of |Er| grows, reaching a maximum at the waveguide boundaries. Further, it can be inferred from the tightly packed contours at the higher propagation constant ($\beta > 15\,\mu m^{-1}$), the field is highly confined as compared to the lower values of propagation constant ($\beta < 10\,\mu m^{-1}$). The contours get wider for lower value, depicting the less confinement. The strong radial electric field near the boundaries could be utilized in sensing or surface-enhanced applications, as the field interacts more significantly with the surrounding environment. Moreover, the careful selection of field distributions and propagation constants can be employed to optimize and design thermo-optical waveguides. As provided in the figures 9–10 that the effective mode index can be tuned by tailoring the external frequency, temperature and radius of NW, the impact of these parameters under the variation of frequency and corresponding effective mode index has been presented in the figure 13.

The results illustrated in figure 13 pertain to the behavior of modes both within and outside the waveguide. These findings were derived by examining the electric field distribution as a function of the waveguide radius across different frequencies, alongside their corresponding effective mode indices (N_{eff}). It can be inferred from these results that the as the effective mode index increases the field profile expanded and transformed into the leaky type modes. It is obvious from the figure13(a), at the lower frequency (f = 2.63 THz, Neff = 81.31), the effective mode index is much higher, indicating strong confinement of the modes within the waveguide. This is reflected in the highly localized electric field profile near the waveguide surface. As the frequency increases (f = 4.54 THz, Neff = 26.24), (f = 4.54 THz, Neff = 26.24) & (f = 4.54 THz, Neff = 26.24) the effective mode index decreases. This reduction corresponds to weaker confinement of the modes, with the electric field spreading further away from the waveguide surface as give in figures 13(b)–(d) respectively. Additionally, to understand the effect of temperature on the field profiles, figure 9 shows that as the temperature increases, the effective mode index also increases. This suggests that higher temperatures lead to stronger confinement of the waveguide modes compared to lower temperatures. The computed results highlight a gradual decrease in Neff

with increasing frequency, indicating a transition in the characteristics of the guided modes. The fields extend farther from the surface, suggesting that the modes become less confined within the waveguide structure.

4. Concluding remarks

This study presents a comprehensive analysis of the fiber modes supported by thermo-optical waveguides utilizing graphene-wrapped InSb nanowires. Using numerical solutions of the characteristic equation through Mathematica, we analyzed the propagation characteristics of graphene-wrapped InSb nanowires, focusing on the effective mode index, propagation band, threshold frequency, and propagation losses under varying temperature, waveguide radius, and chemical potential conditions. The findings indicate a notable temperature dependence, with InSb shifting from an insulating state at 200 K to a conducting state at higher temperatures. This transition significantly impacts the propagation characteristics, demonstrated by contrasting trends in propagation constants and damping features at different temperatures. Additionally, our analysis shows that increasing the chemical potential of graphene produces varied effects on the propagation characteristics, emphasizing the distinct behaviors of waveguide modes in both insulating and conducting states. The effects of waveguide dimensions were also examined, revealing that larger waveguide radii lead to a decrease in the effective mode index and shifts in cutoff frequency. This relationship highlights the importance of structural parameters in optimizing waveguide performance. Ultimately, this research improves our understanding of the intricate interactions between temperature, chemical potential, and structural dimensions in graphene-wrapped InSb nanowire waveguides, offering valuable insights for future photonic device applications.

Authors' contributions

M Sajid and M Z Yaqoob wrote main manuscript and derived analytical expressions. Majeed A S. Alkanhal and Abdul Ghaffar edited the manuscript and reviewed the numerical analysis., Ahtisham Ali and Yasin developed methodology and analysis of results and discussion in the given study. All authors reviewed the manuscript before submission.

Acknowledgments

This work was supported by the Researchers Supporting Project number (RSPD2025R985), King Saud University, Riyadh, Saudi Arabia.

Data availability statement

All data that support the findings of this study are included within the article (and any supplementary files).

ORCID iDs

Muhammad Zeshan Yaqoob https://orcid.org/0000-0001-9145-8604
Majeed A S Alkanhal https://orcid.org/0000-0003-3673-0411
Ahtisham Ali https://orcid.org/0009-0008-8052-1346

References

[1] Pang X, Ozolins O, Jia S, Zhang L, Schatz R, Udalcovs A, Bobrovs V, Hu H, Morioka T and Sun Y-T 2022 Bridging the terahertz gap: photonics-assisted free-space communications from the submillimeter-wave to the mid-infrared *J. Lightwave Technol.* **40** 3149–62
[2] Shen S, Liu X, Shen Y, Qu J, Pickwell-MacPherson E, Wei X and Sun Y 2022 Recent advances in the development of materials for terahertz metamaterial sensing *Adv. Opt. Mater.* **10** 2101008
[3] Gong A, Qiu Y, Chen X, Zhao Z, Xia L and Shao Y 2020 Biomedical applications of terahertz technology *Appl. Spectrosc. Rev.* **55** 418–38
[4] Akyildiz I F, Jornet J M and Han C 2014 Terahertz band: next frontier for wireless communications *Physical Communication* **12** 16–32
[5] Song H-J and Lee N 2021 Terahertz communications: challenges in the next decade *IEEE Transactions on Terahertz Science Technology* **12** 105–17
[6] Carnio B N, Moutanabbir O and Elezzabi A Y 2023 Nonlinear photonic waveguides: a versatile platform for terahertz radiation generation (a review) *Laser Photonics Reviews* **17** 2200138
[7] Shi L-F, Zahid A, Ren A, Ali M Z, Yue H, Imran M A, Shi Y and Abbasi Q H 2023 The perspectives and trends of THz technology in material research for future communication-a comprehensive review *Phys. Scr.* **98** 065006
[8] Tan Z, Zhang Q Y, Lei Y L, Zhao Y and Ding J Q 2023 Terahertz waveguide multiplexers: a review *Microwave Optical Technology Letters* **65** 1925–35

[9] Katyba G, Zaytsev K, Dolganova I, Chernomyrdin N, Ulitko V, Rossolenko S, Shikunova I and Kurlov V 2021 Sapphire waveguides and fibers for terahertz applications *Progress in Crystal Growth Characterization of Materials* **67** 100523
[10] Guo T and Argyropoulos C 2021 Recent advances in terahertz photonic technologies based on graphene and their applications *Advanced Photonics Research* **2** 2000168
[11] Depine R A 2016 *Graphene Optics: Electromagnetic Solution Of Canonical Problems* (Morgan & Claypool Publishers)
[12] Saeed M, Ghaffar A, Rehman S U, Naz M Y, Shukrullah S and Naqvi Q A 2022 Graphene-based plasmonic waveguides: a mini review *Plasmonics* **17** 901–11
[13] Ye L, Sui K, Liu Y, Zhang M and Liu Q H 2018 Graphene-based hybrid plasmonic waveguide for highly efficient broadband mid-infrared propagation and modulation *Opt. Express* **26** 15935–47
[14] Zheng K, Yuan Y, Zhao L, Chen Y, Zhang F, Song J and Qu J 2019 Ultra-compact, low-loss terahertz waveguide based on graphene plasmonic technology *2D Mater.* **7** 015016
[15] Kim J T, Choe J-H, Kim J-S, Seo D, Kim Y D and Chung K H 2018 Graphene-based plasmonic waveguide devices for electronic-photonic integrated circuit *Optics Laser Technology* **106** 76–86
[16] Zhang Y, Wu J, Jia L, Qu Y, Yang Y, Jia B and Moss D J 2023 Graphene oxide for nonlinear integrated photonics *Laser Photonics Reviews* **17** 2200512
[17] Gao Y, Ren G, Zhu B, Liu H, Lian Y and Jian S 2014 Analytical model for plasmon modes in graphene-coated nanowire *Opt. Express* **22** 24322–31
[18] Gao Y, Ren G, Zhu B, Wang J and Jian S 2014 Single-mode graphene-coated nanowire plasmonic waveguide *Opt. Lett.* **39** 5909–12
[19] Chen B, Meng C, Yang Z, Li W, Lin S, Gu T, Guo X, Wang D, Yu S and Wong C W 2014 Graphene coated ZnO nanowire optical waveguides *Opt. Express* **22** 24276–85
[20] Gao Y and Shadrivov I V 2016 Nonlinear coupling in graphene-coated nanowires *Sci. Rep.* **6** 38924
[21] Yu P, Fesenko V I and Tuz V R 2018 Dispersion features of complex waves in a graphene-coated semiconductor nanowire *Nanophotonics* **7** 925–34
[22] Golestanizadeh T, Zarifi A, Jalali T, Maack J R and Wubs M 2019 Hydrodynamic acoustic plasmon resonances in semiconductor nanowires and their dimers *JOSA* B **36** 2712–20
[23] Zhou Y, Chen R, Wang J, Huang Y, Li M, Xing Y, Duan J, Chen J, Farrell J D and Xu H 2018 Tunable low loss 1D surface plasmons in InAs nanowires *Adv. Mater.* **30** 1802551
[24] Zhang C, Liu Y, Li J, Wu Q and Li M 2024 Design of a highly sensitive terahertz temperature and refractive index composite sensor based on an InSb–Ag composite grating *JOSA* B **41** 411–20
[25] Yaqoob M, Ahamd M, Ghaffar A, Razzaz F, Saeed S and Alanazi T 2023 Thermally tunable electromagnetic surface waves supported by graphene loaded indium antimonide (InSb) interface *Sci. Rep.* **13** 18631
[26] Zhou Q, Qiu Q and Huang Z 2023 Graphene-based terahertz optoelectronics *Optics Laser Technology* **157** 108558
[27] Chen X, Tian Z, Li Q, Li S, Zhang X, Ouyang C, Gu J, Han J and Zhang W 2020 Recent progress in graphene terahertz modulators *Chin. Phys.* B **29** 077803
[28] Yaqoob M, Anwar M, Ghaffar A, Alkanhal M A, Khan Y and Shahid M 2024 Temperature-assisted electromagnetic surface modes in graphene-based temperature sensitive metafilms *Optics Continuum* **3** 714–31
[29] Zainud-Deen S H, Malhat H A E-A and El-Refaay E A A 2020 InSb based microstrip patch antenna temperature sensor for terahertz applications *Wirel. Pers. Commun.* **115** 893–908
[30] Chen H, Lai K W C, Sun X, Xi N and Meyyappan M 2012 Indium antimonide (InSb) nanowire-based photodetectors *in Nano Optoelectronic Sensors and Devices* (Elsevier) 209–24
[31] Xu T, Wang H, Chen X, Luo M, Zhang L, Wang Y, Chen F, Shan C and Yu C J N 2020 Recent progress on infrared photodetectors based on InAs and InAsSb nanowires *Nanotechnology* **31** 294004
[32] Mittendorff M, Li S and Murphy T E J A P 2017 Graphene-based waveguide-integrated terahertz modulator *Acs Photonics* **4** 316–21